01 Jun 2019

# Analysis of Geometric Accuracy and Thickness Reduction in Multistage Incremental Sheet Forming using Digital Image Correlation

Mercedes M. Gonzalez

Nathan A. Lutes

Joseph D. Fischer

Mitchell R. Woodside

*et. al. For a complete list of authors, see https://scholarsmine.mst.edu/mec_aereng_facwork/4333*



## Recommended Citation

M. M. Gonzalez et al., "Analysis of Geometric Accuracy and Thickness Reduction in Multistage Incremental Sheet Forming using Digital Image Correlation," *Procedia Manufacturing*, vol. 34, pp. 950-960, Elsevier B.V., Jun 2019.
The definitive version is available at https://doi.org/10.1016/j.promfg.2019.06.105

Available online at www.sciencedirect.com

ScienceDirect

Procedia Manufacturing 34 (2019) 950–960

Procedia MANUFACTURING

www.elsevier.com/locate/procedia

47th SME North American Manufacturing Research Conference, Penn State Behrend Erie, Pennsylvania, 2019

# Analysis of geometric accuracy and thickness reduction in multistage incremental sheet forming using digital image correlation

Mercedes M. Gonzalez , Nathan A. Lutes, Joseph D. Fischer, Mitchell R. Woodside, Douglas A. Bristow*, Robert G. Landers

*Missouri University of Science and Technology, 400 W 13th St. Rolla, MO. 65409*

* Corresponding author. Tel.: +1-573-341-6559. *E-mail address:* dbristow@mst.edu

**Abstract**

Incremental Sheet Forming (ISF) is a freeform manufacturing method whereby a 3D geometry is created by progressively deforming a metal sheet with a single point tool following a defined trajectory. The thickness distribution of a formed part is a major consideration of the process and is believed to be improved by forming the geometry in multiple stages. This paper describes a series of experiments in which truncated cone geometries were formed using two multistage methods and compared to the same geometry formed using the traditional single stage method. The geometric accuracy and thickness distributions, including 3D thickness distribution plots, of each are examined using digital image correlation (DIC). The data collected indicate that multistage forming, compared to single stage forming, has a significant effect on the geometric accuracy of the processed sheets. Moreover, the results of the experiments conducted in this paper show that sheets processed with multistage forming do not have a uniform sheet thickness reduction, rather they have a parabolic-like thickness distribution in the processed region.



*Keywords:* incremental sheet forming, multistage, digital image correlation, strain, thickness, geometric accuracy

## 1. Introduction

Incremental Sheet Forming (ISF) is a modern manufacturing process in which a geometry is formed gradually by inducing a local strain on a flat sheet of metal. This process is advantageous for creating small batches of custom parts or for rapid prototyping and can be a suitable alternative to die-forming due to increased efficiency, cost reduction, and increased forming limitations [1].

Historically, ISF has been conducted in what is referred to as single-stage forming, where a tool path is generated from the desired part geometry and the form is completed in one tool pass. This method has proven to yield poor geometric accuracy and formability, especially with steep forming angles due to high strain concentrations [2]. A different technique to improve the formability and geometric accuracy of parts is to use intermediate geometries to extend the forming limits of single stage forming by shifting the distribution of material in the sheet towards zones of high strain [1].

This method of approaching the final geometry into several intermediate forming steps is referred to as multistage incremental forming (MSIF). Many literatures detail efforts to optimize aspects of MSIF to achieve geometries and thickness distributions previously unrealizable in single stage ISF. Typically, this involves novel tool path strategies or predictive modelling. Skjoedt et al. [1] reports a mixed tool-path strategy allowing the forming of a cup with 90˚ walls. Malhotra et al. [3] proposed a mixed tool-path strategy to increase geometric accuracy by eliminating stepped features that are a byproduct of multi-stage forming. Shi et al. [4] did a study comparing the


10.1016/j.promfg.2019.06.105

effects of various forming strategies on the forming limits of geometries containing vertical features. Duflou et al. [5] studied how the process limitations of ISF could be improved by employing multistage methodologies.

Modelling work has been done by various parties as well in attempts to predict important characteristics of multi-stage forming. Nirala et al. developed an approach to eliminate the stepped features commonly found in multistage forming using FEA software [6]. Li et al. [7] developed an algorithm predicting the number of intermediate stages necessary for a desired thickness distribution and verified it using FEM simulation. Shamsari et al. found that multistage forming may lead to a more uniform thickness distribution, according to FE simulations [8]. Cao et al. [9] developed an algorithm for multi stage thickness prediction and compared the results to two popular prediction methods. It was found that this algorithm was faster and more accurate than previous methods. Li et al. [10] did a study on how different forming parameters affected geometric accuracy of a part and formulated a model to predict the geometric deviation at any point on the form. Cui et al. [11] developed an analytical model for predicting strain distributions throughout a part. This model was validated using numerical simulation as well as experimentally using Digital Image Correlation technology. Furthermore, Mengling modeled vertical parts formed using multistage forming and addressed FEA strain distribution results [13].

Multistage forming has thus been the subject of intense study in the manufacturing world. A major prospect is that improved geometric accuracy and uniform thickness distribution can be achieved by deforming a larger portion of material and by changing the strain distribution of the deformation area [4]. This work implements two multistage forming methods and compares the geometric accuracy of the resulting processed sheets to those formed by a traditional single stage forming method. The results of this work demonstrate that multistage methods have negligible effects on the accuracy of the region within the form path but result in significant geometric changes outside of that region. Furthermore, the sheet thickness data indicate that multistage forming generates a less uniform thickness distribution when compared to that of single stage forming.

**Nomenclature**

| | |
|---|---|
| $t_c$ | Calculated sheet thickness (mm) |
| $t_o$ | Unformed sheet thickness (mm) |
| $e$ | Displacement error (mm) |
| $e_{rms}$ | Root mean squared displacement error (mm) |
| $Z_m$ | Measured displacement in z-direction (mm) |
| $Z_{ref}$ | Reference displacement in z-direction (mm) |
| $\varepsilon_1$ | First principle strain |
| $\varepsilon_2$ | Second principle strain |
| $TR$ | Thickness ratio |
| $N$ | Number of points |

## 2. Background

The displacement and strain data collected in this work was gathered using a Digital Image Correlation (DIC) system. DIC has been used in past literatures to study the deformation and strain of parts undergoing incremental forming. Decultot et al. [12] used DIC to investigate strain fields that were the result of forming different geometries. The effects of different parameters such as complex tool paths, varying step sizes, and different punch diameters were also explored. As mentioned above, Cui et al. [11] used DIC in verifying a strain prediction model. Eyckens et al. [2] used DIC to study the strain behavior of the process and to validate predictions from numerical simulations. This paper used DIC to determine the strain distribution of the sheet after forming and subsequently calculate the sheet thickness.

The principal strains, $\varepsilon_1$ and $\varepsilon_2$, can be extracted from the DIC system and used to calculate the sheet thickness reduction ratio. An ideally formed sheet has uniform thickness after forming, therefore the advantage of understanding the thickness distribution of a formed part is to be able to identify the features of the form which produce the greatest thickness reduction. Parts to be manufactured via incremental sheet forming would have sheet thickness specifications, thus the points of significant thickness reduction indicate points of failure, in other words the sheet thickness does not meet specification. Consequently, validation of thickness prediction based on strain allows conclusions to be drawn about the sheet thickness using DIC data.

The sheet thickness is determined using the thickness ratio, defined by

$$t_c = TR \times t_o, \tag{1}$$

where $t_o$ = 1.5 mm is the original thickness and the TR is the thickness ratio, derived from the Green-Lagrange definition for strain and the volume constancy law [14], given by

$$TR = \frac{1}{\sqrt{2\varepsilon_1 + 1}\sqrt{2\varepsilon_2 + 1}}. \tag{2}$$

Thus, using the first and second principle strains, the thickness at any point in the area of interest can be calculated. DIC technology has been known to accurately measure strains up to 1000% with a resolution of ±0.015 pixels [15]. The uncertainty in the strain calculation was quantified by measuring the range of calculated strains in an unformed sheet. The average two sigma confidence in the first and second principal strains, used to calculate the thickness in this work, are 63.1 με and 84.7 με, respectively.

To validate the thickness calculation, one single stage formed sheet and one multistage formed sheet were cut in half and the thickness at specified locations along the center of the form was measured using a point micrometer. The principle strain values were extracted to calculate the thickness at each point. The measurements were matched with the corresponding calculated values in the DIC software as shown in Figure 1 and Figure 2.

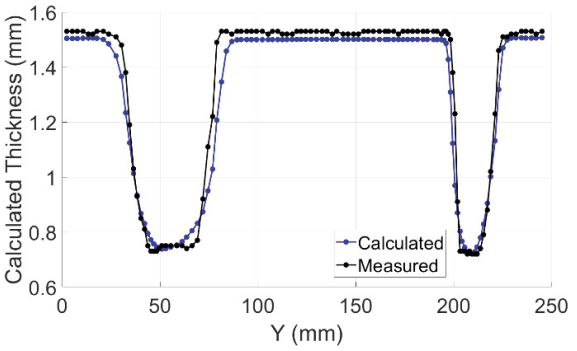


Figure 1. Calculated vs. Measured Thickness, Single Stage

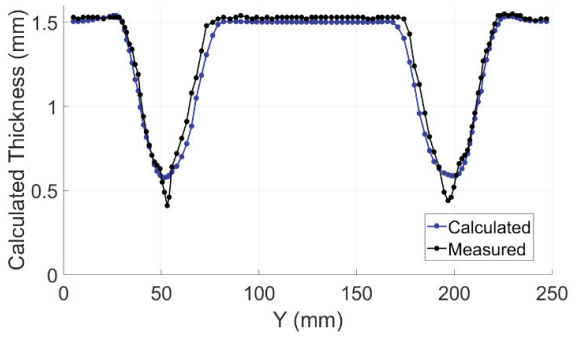


Figure 2. Calculated vs. Measured Thickness, 5 Stage

As shown in Figure 1 and Figure 2, the calculated thicknesses closely align with the measured thicknesses for regions of the form that are unstrained, where the thickness is near the initial thickness of the sheet, around 1.5 mm. To evaluate the accuracy in the DIC, the calculated versus measured thicknesses are compared over the processed region. For Figures 1 and 2, this region is 30 – 80 mm and 170 – 220 mm. The mean absolute difference of the calculation from the measurement in the processed region are 0.05 mm and 0.07 mm for the single stage and 5-stage forms, respectively, and standard deviations of 0.06 mm and 0.04 mm providing a two sigma confidence of 0.17 mm and 0.15 mm for the calculated thickness for single and multistage forms.

At the location where the cone's sidewall meets the truncated diameter, there is a high rate of change of strain because the tool path ends at this interface and the unformed area of the sheet remains unstrained. Thus, the strain changes from nearly 0 on the truncated surface to a location of high strain along the sidewall of the cone. This elevated rate of strain along the truncated edge does not yield accurate thickness micrometer measurements due to the error in the precise location of the measured thickness of the part. Overall, there is a strong correlation between the measured and calculated thicknesses for both parts, therefore validating the use of the thickness ratio to predict sheet thickness using DIC strain data.

## 3. Experimental Setup

### *3.1. Tooling and Data Collection*

The ISF process was implemented using an ABB IRB 940 Tricept robot equipped with a 6.35 mm (1/4") radius spherical steel forming tool. Aluminum 6061-O sheets with nominal dimensions of 457.2×457.2×1.587 mm (18"×18"×1/16") were fastened between two aluminum frames (see Figure 3). The forming area is a 254×254 mm (10"×10") square centered in the frame. To reduce the effects of friction on the form, a layer of 6315 Monolec Way lubricant was applied to the sheet before each form.

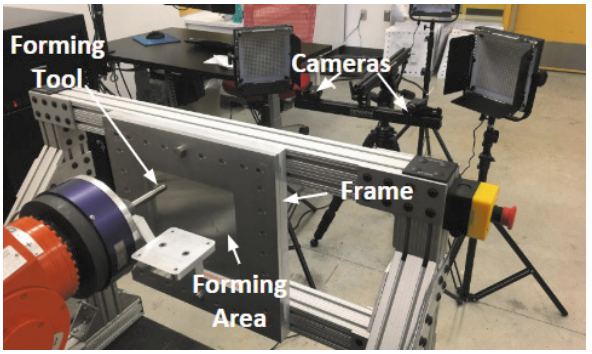


Figure 3. Experimental Setup

Data were collected using a Digital Image Correlation (DIC) system from Correlated Solutions in conjunction with Vic3D software. The DIC system acquired data using two cameras. These cameras captured images of the sheet during the forming process. In order for the DIC system to extract displacement and strain data, the sheets were painted white using matte spray paint and printed with a pseudo-random pattern of black dots (i.e., speckle pattern) as shown in Figure 4. The DIC system used this speckle pattern to identify unique points on the sheet and track their displacements and strains during the forming process.

The DIC system processed the images using the Vic3D software. This software has the capability to measure 3D displacements and strains at each point on the speckle pattern, as well as to calculate the sheet thickness at each point. The extracted data are exported to MATLAB for post processing.

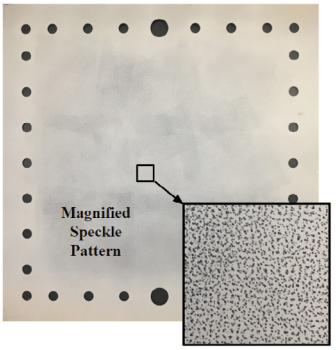


Figure 4. Speckled Aluminium Sheet

Several system parameters can affect the noise and bias in the images, such as lighting, focus, aperture, stereo-angle, and the speckle pattern [12]. While these parameters present limitations to the DIC system, they can be optimized to collect accurate data for the incremental sheet forming process. Multiple LED studio lights are employed to light the area of interest to increase the contrast of the speckle pattern and, thus, reduce the amount of uncertainty when correlating the images. The cameras are focused on the unformed sheet so that clear, distinct features on the part can be identified in the images. Large apertures make the images brighter, however decrease the depth of field. Therefore, given the system used in this work, an aperture of f/6 is used in both cameras to allow adequate light to reach the camera's sensor without overexposing the images. The stereo-angle (i.e., the angle at which the cameras are oriented with respect to the part) and focal length (i.e., the distance from the cameras to the sensor plane) significantly impact the measurement noise. For focal lengths of 35 mm or greater, a stereo angle of no less than 15° is recommended to reduce the amount of noise. This work uses a focal length of about 940 mm (37") and a stereo angle of 23° to obtain adequate data along the sidewalls of the cones. In order to quantify the error in the DIC calculation of displacement and strain, the DIC software calculates the uncertainty at every point on the speckle pattern. The forms in this work yield an average two sigma confidence in the accuracy of the DIC measurements of 0.004 mm for displacement and 0.010 pixels when matching the images from the two cameras.

### *3.2. Form Path*

The form paths were generated using a 3D CAD model of the final desired geometry. The paths consist of a series of closed contours, or layers, at increasing depths. The direction of motion of the tool is reversed after each layer is complete to eliminate local twisting of the sheet. The step depth for each layer was 0.44 mm and the tool speed was 42.5 mm/s.

Figure 5 is an illustration of a simplified tool path for the truncated cone geometry chosen for the forms in this work with arrows indicating the direction of the tool. The tool path was defined to form the sidewalls of the cones; however, not the top truncated surface. The same final geometry is defined for each form in this experiment to compare their geometric accuracies and thickness distributions.

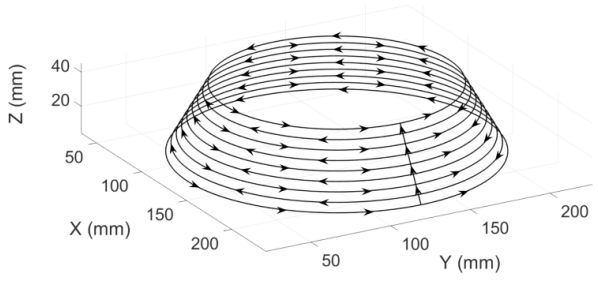


Figure 5. Illustration of Cone Form Path

Four forms were fabricated in this experiment: one single stage form and three multistage forms. Two different methods for generating the intermediate stages of the multistage forms were studied. Method 1 (Forms 2 and 3 shown in Figure 7 and Figure 8, respectively) held the minor diameter, $d_{min}$ = 142.265, constant at each stage and thus the sidewall length increased at each stage. The difference between Forms 2 and 3 was that three and five stages, respectively, were used in the multistage forming process. Method 2 (Form 4 shown in Figure 9) increased the minor diameter of the cone at each stage, while controlling the angle of the sidewall and the height of the cone.

Form 1 (Figure 6) was a single stage form, used to establish a baseline for geometric error and thickness distribution. The major diameter, $d_{maj}$ = 200 mm, is centered in the forming area. The sidewall angle, Θ, measured from the flat sheet is 60°, and the final height $h$ is 50 mm.

Form 2 (Figure 7) consisted of 3 stages using Method 1. Form 2 steps the cone wall angle 20° with each stage, and the depth is calculated to hold the minor diameter, $d_{min}$ = 142.265 mm, constant for each stage. The geometric dimensions of each stage for Form 2 are summarized in Table 1.

Table 1. Form 2 Geometric Dimensions

| Stage | Angle | Height (mm) |
|---|---|---|
| 1 | 20° | 10.506 |
| 2 | 40° | 24.222 |
| 3 | 60° | 50 |

Form 3 (Figure 8) consisted of 5 stages using Method 1. The Five Stage Method 1 form steps the cone wall angle 12° with each stage, and the height is calculated to hold the minor diameter constant for each stage. The dimensions of form 3 are summarized in Table 2.

Table 2. Form 3 Geometric Dimensions

| Stage | Angle | Height (mm) |
|---|---|---|
| 1 | 12° | 6.135 |
| 2 | 24° | 12.852 |
| 3 | 36° | 20.973 |
| 4 | 48° | 32.061 |
| 5 | 60° | 50 |

Form 4 (Figure 9) consisted of 5 stages using Method 2. This method controlled the sidewall angle and height, thus allowing the minor diameter to vary with each stage. As a result, the sidewall length, $l$, ranged from 48 to 58 mm.

Table 3. Form 4 Geometric Dimensions

| Stage | Angle | Height (mm) | Truncated Diameter (mm) |
|---|---|---|---|
| 1 | 12° | 10 | 105.907 |
| 2 | 24° | 20 | 110.158 |
| 3 | 36° | 30 | 117.417 |
| 4 | 48° | 40 | 127.967 |
| 5 | 60° | 50 | 142.265 |

Note that the difference between the two methods is the whether the sidewall length (Method 1) or the truncated diameter of the cone (Method 2) was the independent variable for each stage. The motivation behind Method 2 is to determine if maintaining the length of the sidewalls would induce bending in the sidewalls and stretch the top truncated surface.

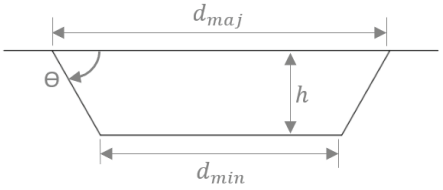


Figure 6. Form 1 -- Single Stage


Figure 7. Form 2 – Three Stage Method 1

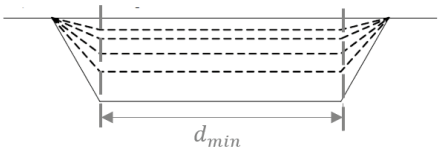


Figure 8. Form 3 – Five Stage Method 1

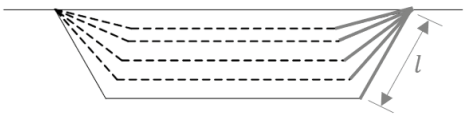


Figure 9. Form 4 – Five Stage Method

## 4. Discussion of Results

### *4.1. Geometric Error*

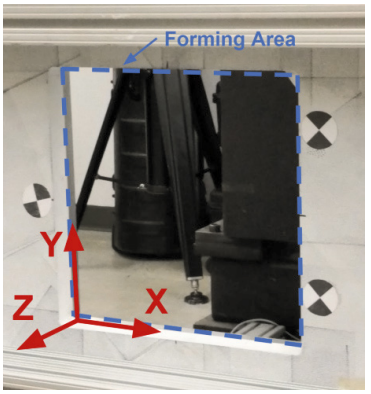


Figure 10. Work Object Coordinate Frame

The coordinate frame origin is defined to be the bottom left-hand corner of the back of the frame, located on the bottom corner of the forming area as shown in Figure 10. The form paths and reference geometries both exist in this coordinate frame. The measured data is collected in the camera coordinate frame originally and later transformed to the work object coordinate frame during post processing. This transformation aligns the measured data with the reference geometry and allows the quantification of the error at each point. The error at the $i^{th}$ point is described as

$$e(i) = z_r(i) - z_m(i), \tag{3}$$

where $z_r$ is the reference displacement (mm) and $z_m$ is the measured displacement (mm). Figure 11 displays an illustration of the error as defined by the reference and measured displacement in the z direction. Positive error values indicate locations of under-forming, whereas negative error values indicate locations of over-forming.

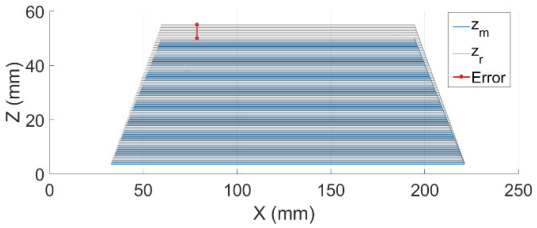


Figure 11. Illustration of Error

Each form in this work contains a pronounced geometric error along the outer edge of the cones. This error is a smoothly curved transition from the base of the plate to the wall of the form as opposed to a sharp angle between the unformed region on the outside of the cone and the boundary of the form path. This smooth transition indicates the local bending occurring around the bottom of the part during forming. As the tool pushes the sheet outwards during the forming process, regions of the sheet not being formed are bending.

An additional large-scale error found in the multistage forms (i.e. Forms 2, 3, and 4) is the change in slope of the sidewall. The first stage defines the slope along the bottom of the cone by bending the material outward with a smooth transition, as previously mentioned. For the following stages, the first few layers do not contact the sheet until a certain depth because the material was over-formed from previous stages. Thus, when the tool makes contact with the sheet, the slope of the sidewall of the cone increases since the angle of each stage is increasing.

Furthermore, Form 4 displays a disc feature along the truncated surface of the cone. These discs are a result of the increasing diameter from the intermediate stages. Since the tool does not re-pass over the points along the inner most diameter, the deformation at those locations is not affected by the rest of the form.

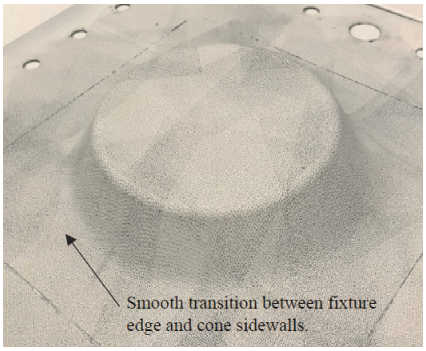


Figure 12. Image of Form 1

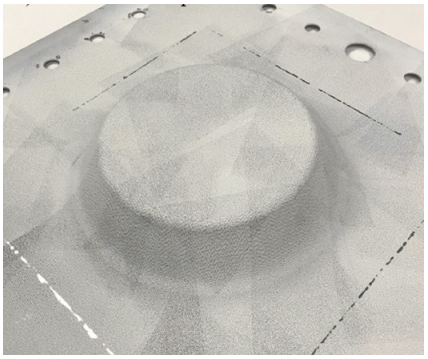

Figure 13. Image of Form 2

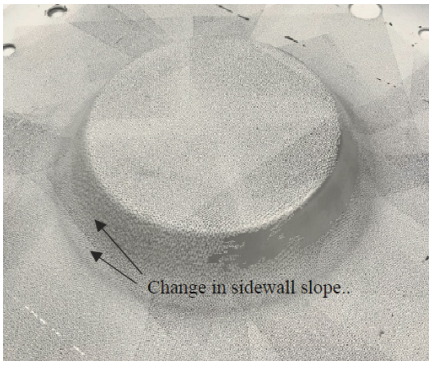


Figure 14. Image of Form 3

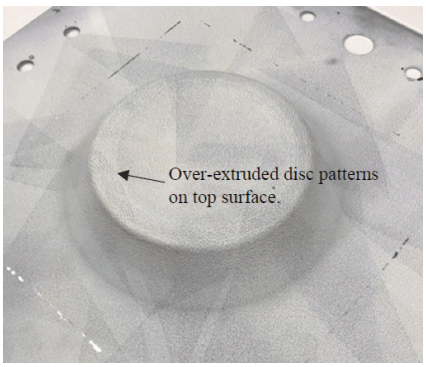


Figure 15. Image of Form 4

To better understand the effects of the multistage forming process on geometry, a cross section of the cone's data was extracted from each form. Figure 16 displays a view of the x-y coordinate plane of the forming area with a form path plotted in black and the location of the selected cross section plotted in blue. The horizontal black line at on the form path indicates the turn-around location where the tool would increment in the z-direction and change directions.

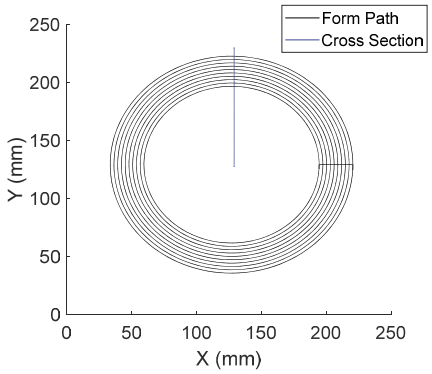


Figure 16. Cross Section on Cone Tool Path

The previously mentioned smooth curved transition is evident in each cross-section deformation plot as shown in Figure 17, in the 95 to 120 mm region. This can be attributed to forming a shape smaller than the forming area, defined in Figure 16 as the range of x and y values from 0 to 254 mm. Additionally, the square boundaries of the frame do not match the circular contour of the formed part, so the difference between their shapes creates a region of the sheet that is not formed by the tool path and thus is not directly controlled.

As shown in the graphs for the nominal (Figure 17) and the Method 1 forms (Figure 18 and Figure 19), the top surface of the cone is under-formed; however, the sidewalls are over-formed. Since the sidewalls are the locations at which the form path is defined, and the final stage form path is based on the reference geometry, there tends to be over forming even for single stage. This occurs because the tool's tip is programmed to move to the coordinate at which the reference geometry is defined, pushing the sheet farther than the reference z-displacement, thus over forming the sheet.

In terms of the error outside of the form path, when increasing the number of stages in a form, as shown by comparing Forms 1, 2, and 3, in Figure 17 - Figure 20, respectively, the bending region of the sheet, along the outer edge of the cone in the range of 95 to 120 mm, tends to bend more with an increased number of stages as shown in Figure 21. This is because as the tool passes over the sheet with each stage, it shears the sections of the sheet it is passing over and bends the material that is unformed at an increasing angle and depth into the form with each stage.

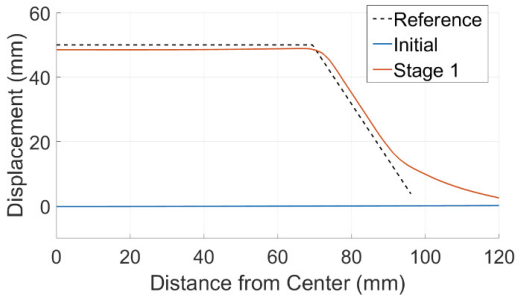


Figure 17. Form 1 Cross Sectional Deformation

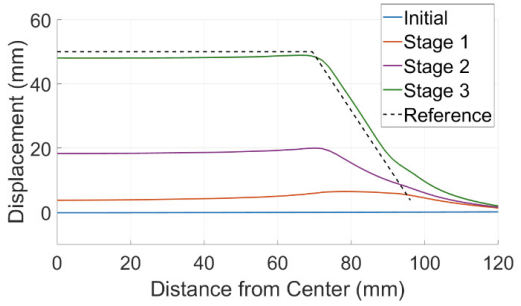


Figure 18. Form 2 Cross Sectional Deformation

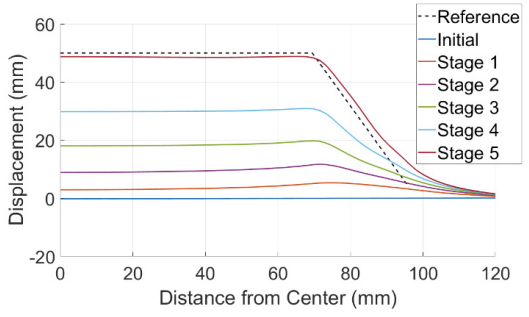


Figure 19. Form 3 Cross Sectional Deformation

Method 2, shown in Figure 20, yielded a more accurate top surface between 50 and 80 mm, due to the aforementioned discs developed during the intermediate stages. Between 0 and 50 mm, where the tool does not pass over the material, the error is closer to the Method 1 forms where the unformed region in the center of the cone does not reach the reference.

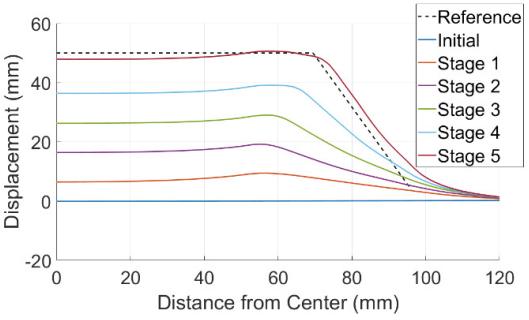


Figure 20. Form 4 Cross Sectional Deformation

The final cross-sectional deformations for each form are plotted with the reference geometry in Figure 21. Both 5 stage forms display less smoothing to the fixture along the outer edge of the cone, in the 95 to 120 mm region.

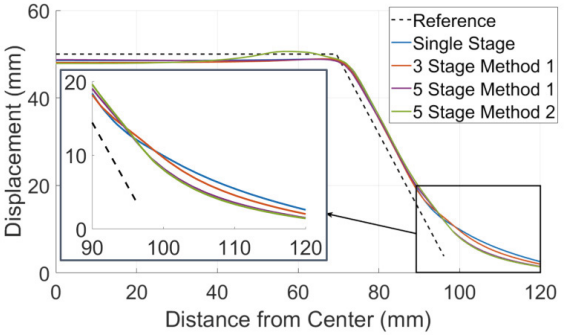


Figure 21. Deformation Comparison of Final Forms

To address the distribution of geometric error, the area of interest was divided into two sections, defined as the formed region and the unformed region, as shown in Figure 22. The formed region is the area of the sheet defined by the x and y coordinates that lie within the major diameter of the cone. The unformed region is the area outside of the formed region, where the tool does not come in contact with the sheet.

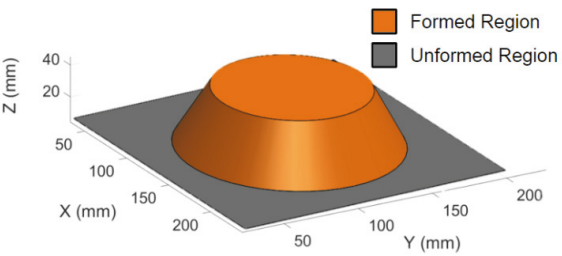


Figure 22. Illustration of Formed and Unformed Region

To analyze the geometric accuracies of the formed parts, the root mean square (RMS) error is used

$$e_{RMS} = \sqrt{\frac{\sum_{i=1}^{N} e(i)^2}{N}}, \tag{4}$$

where $N$ is the total number of data points in the region.

In order to analyze the results of the multistage forms, a study of the repeatability of the process was conducted. The single stage form path was implemented five times, and the results are summarized in Table 4. The average and standard deviation were calculated for each region and displayed at the bottom of Table 4.

Table 4. Geometric Error Repeatability in Single Stage Forming

| Form | Formed Region RMS Error (mm) | Unformed Region RMS Error (mm) |
|---|---|---|
| Form 1a | 4.161 | 7.469 |
| Form 1b | 4.543 | 7.898 |
| Form 1c | 4.038 | 7.314 |
| Form 1d | 3.819 | 7.006 |
| Form 1e | 4.107 | 7.537 |
| Average | 4.133 ± 0.263 | 7.445 ± 0.325 |

The RMS errors for both regions of each multistage form are shown in Table 5. The RMS error values in the formed region for the Method 1 forms (Forms 2 and 3) fall within one standard deviation of the average single stage RMS error, indicating that this multistage method has negligible effects on the formed region of the part. The 5-Stage Method 2 form yielded an RMS error greater than two standard deviations away from the mean. This is due to over-forming in the sidewall region.

Contrarily, the unformed RMS errors in the 5-Stage forms (Forms 3 and 4) are greater than two standard deviations away from the average single stage error. The RMS errors are reduced by 17.0%, and 22.6% for Forms 3 and 4, respectively. These reductions in RMS error demonstrate that the intermediate stages of the 5-Stage methods are bending the sheet around the edges of the cone's major diameter and thus improving geometric accuracy in the unformed region. This effect can be observed in Figure 21, where the deformation of the 5-Stage Method 2 is closest to the reference in the 95 to 120 mm region.

Table 5. Effect of Multistage Forming on Geometric Error

| Form | Formed Region RMS Error (mm) | Unformed Region RMS Error (mm) |
|---|---|---|
| Form 1: Single Stage | 4.133 | 7.445 |
| Form 2: 3-Stage Method 1 | 4.380 | 7.097 |
| Form 3: 5-Stage Method 1 | 4.562 | 6.177 |
| Form 4: 5-Stage Method 2 | 4.729 | 5.765 |

### *4.2. Sheet Thickness*

The DIC data is used to create a 3D model of the calculated thickness. The models for Forms 1–4 are shown in Figure 23 - Figure 26, respectively. There are various instances of missing data scattered across the 3D images of the thickness distribution plots, where the DIC system failed to correlate the image pixels at those locations with the reference image. This is a consequence of the DIC system as it is dependent on adequate, consistent lighting and suitable camera angle for capturing images of the sidewalls of the forms. Therefore, the missing data is a result of the cameras not being able to accurately observe those portions of the form. However, this has no bearing on the accuracy of the remainder of the data which is correlated independently.

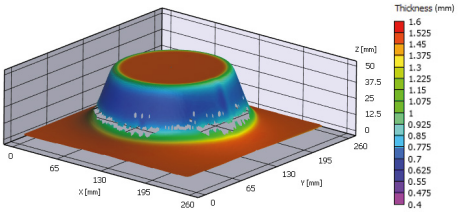


Figure 23. Form 1 - 3D Thickness Model

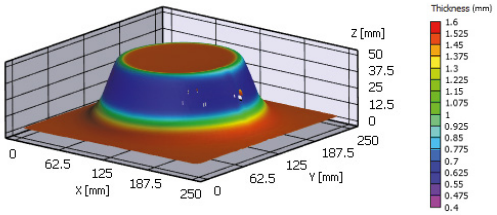


Figure 24. Form 2 - 3D Thickness Model

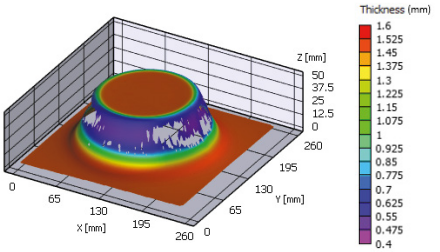


Figure 25. Form 3 - 3D Thickness Model

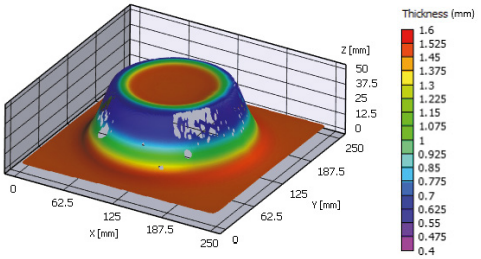


Figure 26. Form 4 - 3D Thickness Model

As shown in these plots, the location of the minimum thickness tends towards the top edge of the sidewall as the number of stages increases. To understand this effect more clearly, the calculated thickness was analyzed along the cross section (from Figure 16) for each form.

The reference geometry is superimposed on the thickness graph to indicate the locations of the sidewall, plotted on the secondary y-axis. The single stage thickness distribution along the sidewall of the cone (Figure 27) resembles a Gaussian distribution, where the top and bottom of the form are the least strained, thus yielding the least amount of thickness reduction, and the middle of the wall is strained the most, yielding the most thickness reduction.

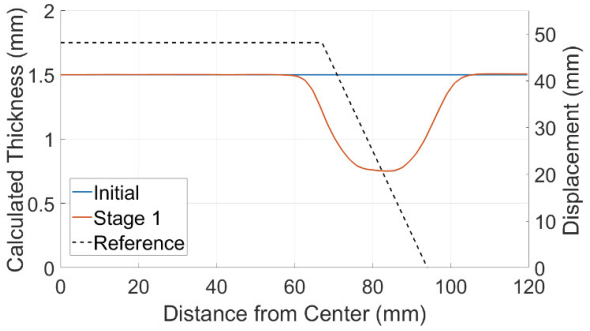


Figure 27. Form 1 Cross Sectional Thickness

Between the 3 Stage Method 1 and the 5 Stage Method 1 forms, as shown in Figure 28 and Figure 29, the thickness distributions are similar.

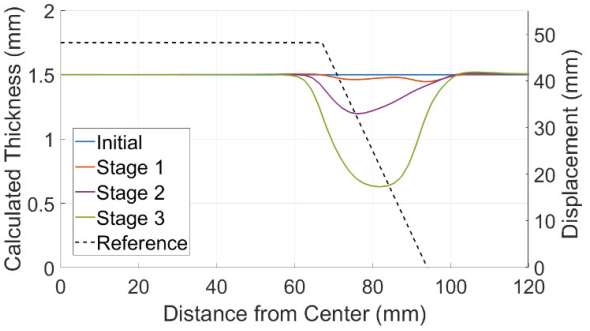


Figure 28. Form 2 Thickness

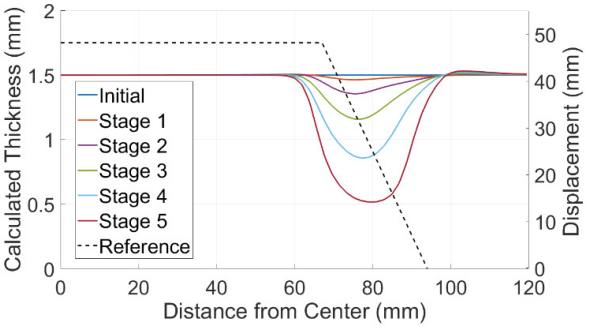


Figure 29. Form 3 Cross Sectional Thickness

A similar phenomenon of minimum thickness propagation occurs with Method 2; however, the location of the minimum thickness at each stage begins towards the center of the form and tends towards the center of the sidewall, as seen in Figure 30. This is because the form paths of the intermediate stages of Method 2 are defined closer to the center of the cone since the minor diameter increases with each stage. Since the minor diameter was changing, the same region on the x-y plane was not strained at each stage, and thus led to less sheet thinning by the final stage.

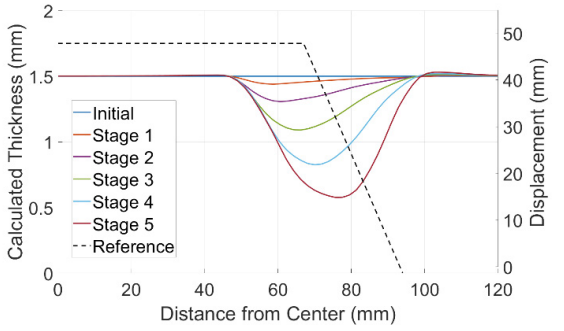


Figure 30. Form 4 Cross Sectional Thickness

The final calculated thicknesses for each form are plotted in Figure 31. The relationship between the number of stages and the minimum sheet thickness for the Method 1 forms indicates that with increased number of stages, the location of minimum sheet thickness tends towards the center of the sidewall. However, for Method 2, with an increased number of stages, the minimum thickness tends towards the location on the form of greatest displacement, in this case near the minor diameter of the truncated cone.

There is a clear difference in the thickness distribution between Methods 1 and 2. In Method 1, the minimum thickness propagates at the same location, approximately in the center of the sidewall as shown in Figure 29. The intermediate stages of the Method 1 forms have the same minor and major diameters, thus defining the form paths in the same region for each stage. As a result, the form path is defined in the same region on the x-y plane for each stage and thus the same region is strained at each stage.

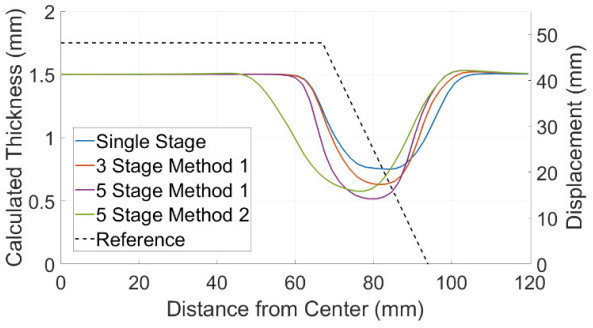


Figure 31. Cross Sectional Thickness Comparison

One interesting aspect of all the thickness graphs occurs beyond the outer edge of the form path. In this region, the methods used to characterize the thickness predict a thickness that is larger than that of the unformed part. However, it is unlikely that the part is truly thicker in this region since this would require a dominant compressive effect, which is widely accepted as infeasible with traditional SPIF processes.

In order to determine the cause of this inaccuracy of the thickness calculation from the DIC measurement, it is important to understand what is taking place in this region. One important characteristic of this region is that it lies outside of the tool path. As such, this region is never contacted by the tooltip, and the result is that this region is not dominated by shearing, but by bending. This effect causes the surface of the sheet – which is measured by the DIC – to be put into slight compression, while the underside which cannot be seen by the DIC is placed under tension.

Since the DIC can only view the outer compressive surface of this region and the thickness formula assumes constant strain throughout the thickness of the part, the formula predicts a part that is thicker than the original. As such, regions that are characterized by a dominant bending effect are outside the scope of this equation.

For all forms in this work, the thickness of the sheet is significantly reduced where the form path is defined. Thus, this particular section is of interest when comparing the sheet thickness distributions of the single stage form to the multistage forms. To compare the uniformity of sheet thickness in the processed region, each calculated thickness in the area of interest less than 1.45 mm is plotted in the histogram shown in Figure 32. The single stage form has the least magnitude of thinning, most recurrently at 0.75 mm. The 5-Stage Method 1 form has the greatest magnitude of thinning from the initial sheet thickness of 1.5 mm, as well as the most frequent amount of thinning to a sheet thickness of 0.51 mm, 0.24 mm less than that of the single stage. The 5-Stage Method 2 form has the next greatest magnitude of thinning, most commonly at 0.58 mm, 0.17 mm less than that of single stage. Both differences are greater than or equal to the aforementioned two-sigma confidence in thickness calculation, 0.17 mm. All three multistage experiments have the greatest frequency of thinning at sheet thicknesses less than the single stage form thinned the sheet at any point. Additionally, the single stage form shows the greatest frequency of any one thickness, indicating the most uniformity, demonstrating that the multistage method of forming can yield a less uniform distribution of sheet thickness when compared to single stage forming.

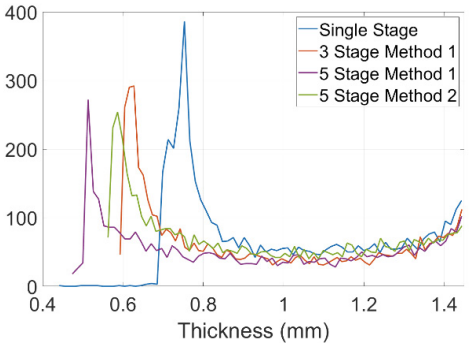


Figure 32. Thickness Distribution Histogram

## 5. Summary and Conclusions

Multistage incremental sheet forming has been a suggested solution for increased formability, improved accuracy, and a more uniform sheet thickness than single stage incremental sheet forming. The results of this work indicate that multistage forming improves the geometric accuracy of the unformed region by bending the sheet outside of the form path. The data also suggest that multistage forming may result in a less uniform sheet thickness than single stage forming in the processed region. Future work on multistage forming should include the investigation of geometric accuracy and sheet thickness distribution for asymmetric geometries to determine if the same conclusions can be made for complex parts. Additionally, a method for defining the intermediate stages should be further explored using digital image correlation to understand the strain during forming and to predict the locations of failure points on steep walled parts.

## Acknowledgements

This work was supported by the Boeing Company and the Center for Aerospace Manufacturing Technologies at the Missouri University of Science and Technology.

## References

[1] M. Skjoedt, N. Bay, B. Endelt, and G. Ingarao, “Multi Stage Strategies for Single Point Incremental Forming of a Cup,” International Journal of Material Forming, vol. 1, no. S1, pp. 1199–1202, 2008.

[2] P. Eyckens, B. Belkassem, C. Henrard, J. Gu, H. Sol, A. M. Habraken, J. R. Duflou, A. V. Bael, and P. V. Houtte, “Strain evolution in the single point incremental forming process: digital image correlation measurement and finite element prediction,” International Journal of Material Forming, vol. 4, no. 1, pp. 55–71, 2010.

[3] R. Malhotra, A. Bhattacharya, A. Kumar, N. Reddy, and J. Cao, “A new methodology for multi-pass single point incremental forming with mixed toolpaths,” CIRP Annals, vol. 60, no. 1, pp. 323–326, 2011.

[4] X. Shi, G. Hussain, G. Zha, M. Wu, and F. Kong, “Study on formability of vertical parts formed by multi-stage incremental forming,” The International Journal of Advanced Manufacturing Technology, vol. 75, no. 5-8, pp. 1049–1053, Oct. 2014.

[5] J. Duflou, J. Verbert, B. Belkassem, J. Gu, H. Sol, C. Henrard, and A. Habraken, “Process window enhancement for single point incremental forming through multi-step toolpaths,” CIRP Annals, vol. 57, no. 1, pp. 253–256, 2008.

[6] Nirala, Harish Kumar, et al. “An Approach to Eliminate Stepped Features in Multistage Incremental Sheet Forming Process: Experimental and FEA Analysis.” Journal of Mechanical Science and Technology, vol. 31, no. 2, 2017, pp. 599–604., doi:10.1007/s12206-017-0112-6.

[7] J. Li, J. Hu, J. Pan, and P. Geng, “Thickness distribution and design of a multi-stage process for sheet metal incremental forming,” The International Journal of Advanced Manufacturing Technology, vol. 62, no. 9-12, pp. 981–988, 2011.

[8] Shamsari, Mohsen, et al. “Formability Improvement in Single Point Incremental Forming of Truncated Cone Using a Two-Stage Hybrid Deformation Strategy.” The International Journal of Advanced Manufacturing Technology, vol. 94, no. 5-8, 2017, pp. 2357–2368., doi:10.1007/s00170-017-1031-5.

[9] T. Cao, B. Lu, D. Xu, H. Zhang, J. Chen, H. Long, and J. Cao, “An efficient method for thickness prediction in multi-pass incremental sheet forming,” The International Journal of Advanced Manufacturing Technology, vol. 77, no. 1-4, pp. 469–483, 2014.

[10] Z. Li, S. Lu, T. Zhang, Z. Mao, and C. Zhang, “Analysis of geometrical accuracy based on multistage single point incremental forming of a straight wall box part,” The International Journal of Advanced Manufacturing Technology, vol. 93, no. 5-8, pp. 2783–2789, Jul. 2017.

[11] Z. Cui, Z. C. Xia, F. Ren, V. Kiridena, and L. Gao, “Modeling and validation of deformation process for incremental sheet forming,” Journal of Manufacturing Processes, vol. 15, no. 2, pp. 236–241, 2013
[12] N. Decultot, L. Robert, V. Velay, and G. Bernhart, “Single point incremental sheet forming investigated by in-process 3D digital image correlation,” EPJ Web of Conferences, vol. 6, p. 11001, 2010.
[13]Wu, Mengling, et al. “FEA of Vertical Parts Formed with Multistage Incremental Sheet Metal Forming Based on the Forming Limit Stress Diagram.” *The International Journal of Advanced Manufacturing Technology*, vol. 93, no. 5-8, 2017, pp. 2155–2160., doi:10.1007/s00170-017-0630-5.
[14] Van Mieghem, B., Ivens, J. & Van Bael, A. Exp Tech (2016) 40: 1409. https://doi.org/10.1007/s40799-016-0143-4
[15] M. Sutton, *Image Correlation for Shape, Motion and Deformation Measurements*. New York: Springer Science+Business Media, 2009, p. 580.